A NUMERICAL METHOD OF 3-D FLOW AROUND SUBMERGED SPUR-DIKES

Yilin ZHOU[1], Masanori MICHIUE[2] and Osamu HINOKIDANI[3]

[1]Student Member of JSCE, Ph. D student, Faculty of Engineering, Tottori University
[2]Fellow of JSCE, Professor, Faculty of Engineering, Tottori University
[3]Member of JSCE, Associate Professor, Faculty of Engineering, Tottori University
(Koyama Cho Minami 4-101, Tottori City, 680-0945, Japan)

A large-eddy simulation tool is adopted to simulate the three-dimensional flow around the submerged spur-dikes. A numerical method is put forward to compute the three-dimensional flow with free surface and complex boundaries. The numerical method is established on the base of finite-volume/finite-difference method with staggered grid. A method of the equivalent Cartesian grid in a fluid cell, whose volume is the same with that of the irregular fluid cell, is used to deal with the irregular cells and the eddy viscosity coefficient at the boundary cells in the flow field with complex boundaries. The water surface and the velocity distribution around submerged spur-dikes of simulation are compared with those of experiment. It is shown that the results of simulation are in agreement with those of experiment and it is possible to apply the numerical model to simulate the complex flow with complex boundaries.

Key Words: *Large-eddy simulation, finite-volume method, three-dimensional flow, spur-dike, Cartesian coordinate, staggered grid*

1. INTRODUCTION

In the past, 3-dimensional Reynolds-averaged Navier-Stokes (RANS) equations were made use of to compute the flow field with free surface around spur-dikes[1), 2), 3)]. A certain difference exists between computation and experiment. The comparison between the water surface of simulation and that of experiment was not made[3)]. For problems with medium to large deformations the numerical methods produce results that are reasonable from a physical viewpoint while their accuracy is difficult to assertain[4)]. For the reason that the flow around a spur-dike is 3-dimensional because of the irregular boundary conditions and strong reverse flows, the shortcomings of RANS equations may explain the difference between computation and experiment.

To solve the difficulty facing to RANS, the large-eddy simulation (LES) is an alternative approach. LES is superior to RANS method when the flow is really complex and especially when large-scale structures dominate the turbulent transport and unsteady process is involved[5)]. Here, we made an attempt to simulate the unsteady 3-dimensional flow with free surface around submerged spur-dike with different angles. Computational results were analyzed and compared with experimental ones. It shows that LES is suitable to be applied to simulate the unsteady flow around spur-dikes.

2. LES EQUATIONS

The LES equations filtered through Navier-stokes equations are written as[6)],

$$\frac{\partial u_l}{\partial t}+u_m\frac{\partial u_l}{\partial x_m}=g_l-\frac{\partial P}{\partial x_l}+\frac{\partial}{\partial x_m}(2\nu_s S_{lm}), \quad (1)$$

where u_l is velocity, g_l is acceleration of gravity, P is pressure, x_l is axis of Cartesian coordinate, $\nu_s=\nu+\nu_t$, $S_{lm}=\frac{1}{2}\left(\frac{\partial u_l}{\partial x_m}+\frac{\partial u_m}{\partial x_l}\right)$.

Smagorinsky (1963) proposed an eddy-viscosity model[7)], which is widely used at present. Smagorisky's eddy viscosity is written as,

$$\nu_t=(C_S\Delta)^2|S|, \quad (2)$$

where C_S is a coefficient, $|S| = \sqrt{2S_{lm}S_{lm}}$, $\Delta = \sqrt[3]{\Delta x \Delta y \Delta z}$, Δx, Δy, Δz are cell sizes in x, y, z directions of Cartesian coordinate. For channel flows, usually $C_S = 0.1$.

The free surface condition is:

$$\frac{\partial h}{\partial t} = w^s - u^s \frac{\partial h}{\partial x} - v^s \frac{\partial h}{\partial y}. \tag{3}$$

where h is water depth from water surface to bed plane, u^s, v^s, w^s are water surface velocities in x, y, z directions, respectively.

3. NUMERICAL METHOD

The equivalent Cartesian grid is utilized to approximate complex geometry and to simulate incompressible fluid flows over complex boundaries. Here we give the equivalent Cartesian grid in the x, y-directions (see Fig.1). In Fig.1, the imaginary lines are grid lines, the fine actual lines are the equivalent Cartesian grid lines and the coarse actual lines are the boundary of the obstacle. As shown in Fig.1, the complex geometry is approximated as both Cartesian grid lines and equivalent Cartesian grid line segments. The conservation of mass and momentum on complex boundaries is enforced by the second-order interpolation or extrapolation method (see Chap. 4).

The finite-difference LES equations were discretized on staggered grid[8), 9), 10)]. The time integration was computed by using the second-order Adams-Bashforth method. For space terms, the second-order centered difference method was used. For pressure term, Projection method was applied to compute pressure and velocities by means of iteration.

4. BOUNDARY CONDITIONS

(1) Water-surface velocities

In the MAC (marker and cell) method, the velocities of two points near the water surface are assumed the same[8)]. Then, it is easy to determine the water surface velocities. In fact, there is a vertical distribution for velocity or pressure. If MAC method is used, it will cause some errors for surface velocities and surface position calculations. Here, we use Lagrangian interpolation or extrapolation method to approximate the vertical distribution of velocity (see Fig.2). The water surface velocities and pressure for the position (i, j) are,

$$u^s_{i+\frac{1}{2},j} = 0.5(1+c_u)c_u u_{i+\frac{1}{2},j,k-2} - (2+c_u)c_u u_{i+\frac{1}{2},j,k-1} + 0.5(2+c_u)(1+c_u)u_{i+\frac{1}{2},j,k}, \tag{4}$$

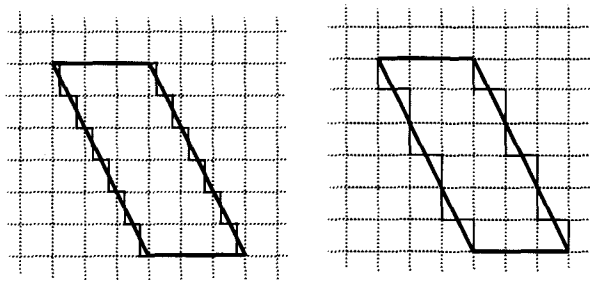

(a) In x-direction (b) In y-direction

Fig.1 The equivalent Cartesian grid

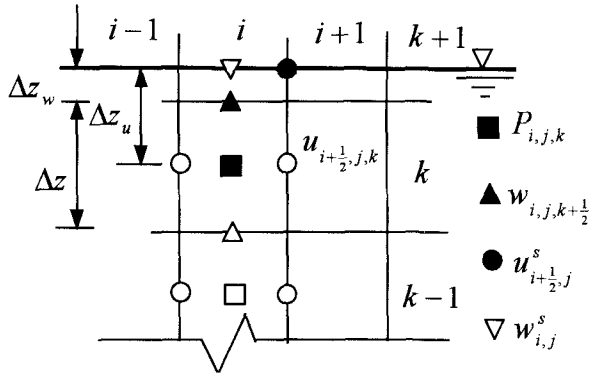

Fig.2 Water surface condition

$$w^s_{i,j} = 0.5(1+c_w)c_w w_{i,j,k-\frac{3}{2}} - (2+c_w)c_w w_{i,j,k-\frac{1}{2}} + 0.5(2+c_w)(1+c_w)w_{i,j,k+\frac{1}{2}}, \tag{5}$$

$$P^s_{i,j} = P_s, \tag{6}$$

where $c_u = \Delta z_u / \Delta z$, $c_w = \Delta z_w / \Delta z$, P_s is water surface pressure.

For the cell above the calculation area, we assume the velocity as (see Fig. 2):

$$u_{i+\frac{1}{2},j,k+1} = u^s_{i+\frac{1}{2},j}, \tag{7}$$

$$w_{i,j,k+\frac{3}{2}} = \begin{cases} w^s_{i,j}, & c_w \geq 0 \\ w_{i,j,k+\frac{1}{2}}, & c_w \leq 0 \end{cases} \tag{8}$$

$$P_{i,j,k+1} = P_s - g(\Delta z - \Delta z_w) \tag{9}$$

Using the method mentioned above, it is not difficult to obtain $v^s_{i,j+\frac{1}{2}}$ and $v_{i,j+\frac{1}{2},k+1}$ (omitted).

It is proved that the water depth and surface velocities computed by this method is more in agreement with experiment than that computed by the original MAC method[10)].

(2) Boundary-cell velocity

The principle to determine the velocities and pressure adjacent to walls is no-slip condition and mass conservation law with which the velocities are

satisfied, respectively. The velocity distribution near the boundary cell is assumed to vary continuously (see Fig.3). Then the second-order interpolation or extrapolation formula to calculate the boundary-cell velocity is obtained as follows.

$$u_0 = (a_1|b| + a_2 b^2)\,sign(b)\,sign(u_1) \qquad (10)$$

where, $a_1 = \dfrac{u_1(2\Delta x + b)^2 - u_2(\Delta x + b)^2}{\Delta x(\Delta x + b)(2\Delta x + b)}$,

$$a_2 = \frac{u_2(\Delta x + b) - u_1(2\Delta x + b)}{\Delta x(\Delta x + b)(2\Delta x + b)},$$

$$sign(b) = \begin{cases} 1 & b > 0 \\ 0 & b = 0 \\ -1 & b < 0 \end{cases}.$$

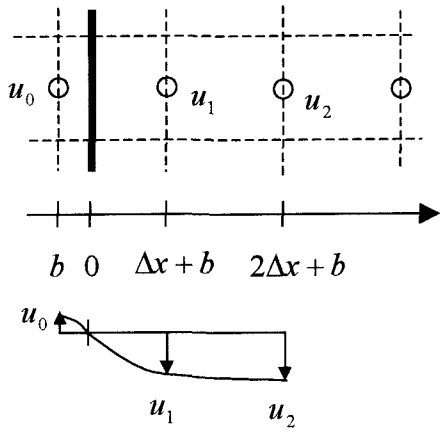

Fig.3 Boundary-cell velocity

(3) Entrance and exit

Velocity distributions of entrance and exit were given at first before computing. From numerical results of water surface, there is a transition before arriving at the real 3-dimensional flow from the position where velocity is given (see Fig.4). In the case of simulation (see Chap.5), Δx_1=50cm, Δx_2=30cm. If the length of simulation is 300cm, the ideal length of simulation results of 3-dimensional flow is about 220cm.

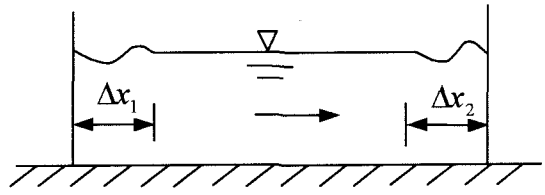

Fig.4 Sketch of simulation reach

(4) Water depth

The finite-difference approximation of equation (3) is written using a space-centered, forward-in-time difference method. For time integration, Adams and Bashforth method is used to compute the time integration of water depth.

For water depth near the boundary, we use Lagrangian extrapolation method to determine water depth value inside the boundary as (see Fig.5),

$$h_0 = 3(h_1 - h_2) + h_3. \qquad (11)$$

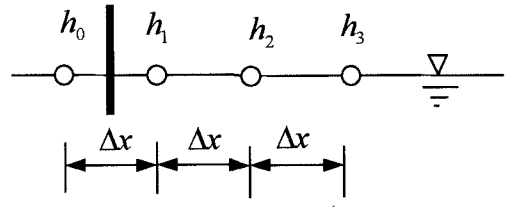

Fig.5 Water depth boundary condition

(5) Eddy viscosity coefficient

Usually, the eddy viscosity coefficient is calculated by using damping functions, such as Van Driest's equation [11]. It requires fine-grid arrangement at the boundary and expensive calculation. To avoid the defects of the former method, the eddy viscosity coefficient in a cell is determined according to the fluid volume inside it. Here we give the following formula to compute the eddy viscosity coefficient with full fluid or partial fluid (see Fig.6):

$$\nu_{tb} = (fC_S\Delta)^2|S| \qquad (12)$$

where $f = V_P/V_F$, V_P is the cell volume with partial fluid, V_F is the cell volume with full fluid. If

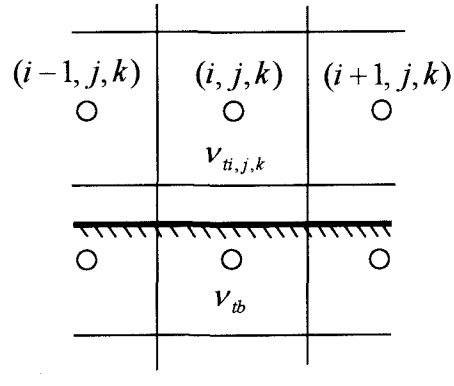

Fig.6 Boundary-cell for ν_{tb}

a cell is full of fluid, the eddy viscosity coefficient calculated from equation (12) is the same with that calculated from equation (2).

5. VERIFICATION

The experiment was carried out in an 18.5m long, 0.4m wide and 0.4m deep flume. The flow discharge is $0.015m^3/s$ and the water depth of uniform flow is 0.1m. A submerged spur-dike was set in the middle of flume. The submerged spur-dike is 0.1m long in the cross-section, 0.05m high, and 0.015m thick. The experiment was carried out with two kinds of spur-dike. One is 60-degree spur-dike (repelling spur-dike) and another is 120-degree spur-dike (attracting spur-dike). The observing reach for experiment is 200cm long and the spur-dike is set at x=100cm[12]. The simulation of 3-D flow was carried out with $300\times42\times15$ grids and each of grid sizes is 0.01m. The water surface and the velocity distribution of simulation are compared with those of experiment.

(1) Water surface

For longitudinal direction or lateral direction, there is a section where the water surface varies more greatly than other sections. Here we choose the longitudinal section (y=4cm) and the cross-section (x=110cm) to compare the water surface of simulation with that of experiment.

a) The longitudinal section

The phenomenon of water surface in the longitudinal section is that the water surface at first goes up slowly until x=90cm; then the water surface goes down fast until x=105cm for the condition of 60-degree spur-dike or x=110cm for the condition of 120-degree spur-dike. From the lowest point the water surface goes up again. The upstream water surface until spur-dike of simulation is the same with that of experiment for both the condition of 60-degree spur-dike and the condition of 120-degree spur-dike (see Fig.7). From x=100cm to x=140cm, the water surface of simulation is a little different from that of experiment. The maximum difference is 4.0mm for the condition of 60-degree spur-dike and 3.2mm for the condition of 120-degree spur-dike. However, from x=150cm the result of simulation is almost the same with that of experiment.

b) The cross-section

The phenomenon of the water surface in the cross-section is that the water surface (y<15cm) is lower than the water surface (y>15cm). In the area (y<15cm), the water surface of simulation is higher than that of experiment (see Fig.8). The

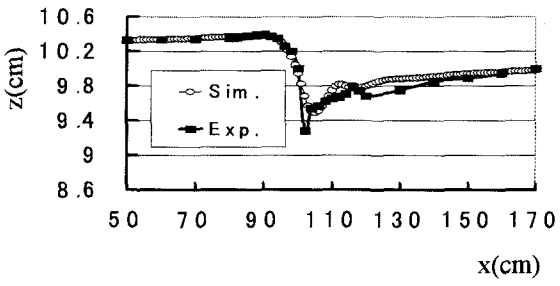

(a) 60-degree spur-dike (y=4cm)

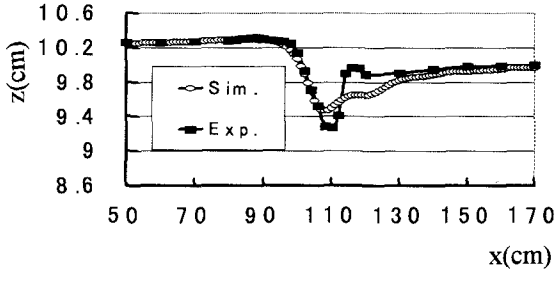

(b) 120-degree spur-dike (y=4cm)

Fig.7 Water surface in the longitudinal section

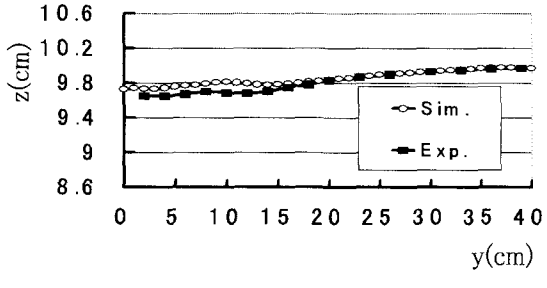

(a) 60-degree spur-dike (x=110cm)

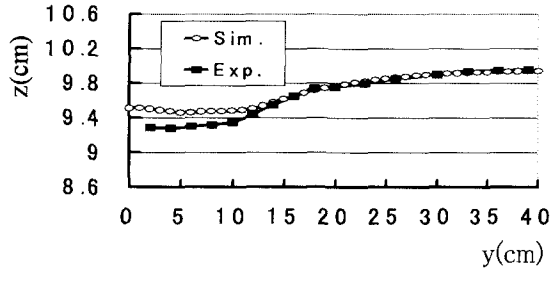

(b) 120-degree spur-dike (x=110cm)

Fig.8 Water surface in the cross-section

maximum difference is 1.3mm for the condition of 60-degree spur-dike and 2.5mm for the condition of 120-degree spur-dike. From y=15cm to y=40cm, the water surface of simulation is the same with that of experiment for both the condition of 60-degree spur-dike and the condition of 120-degree spur-dike.

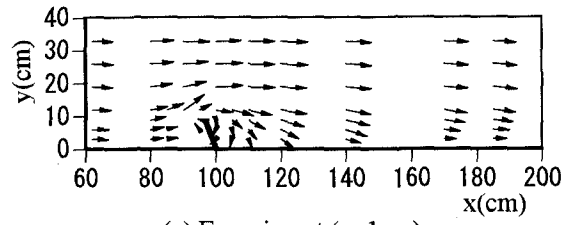

(a) Experiment (z=1cm)

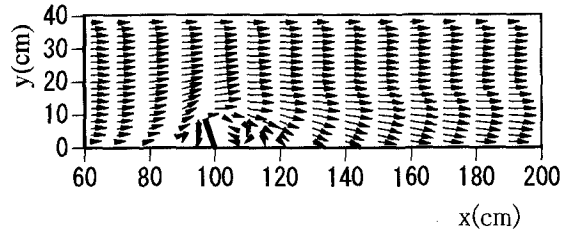

(b) Simulation (z=1cm)

Fig.9 60-degree spur-dike

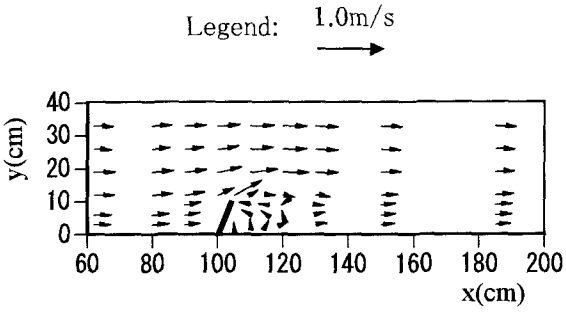

(a) Experiment (z=1cm)

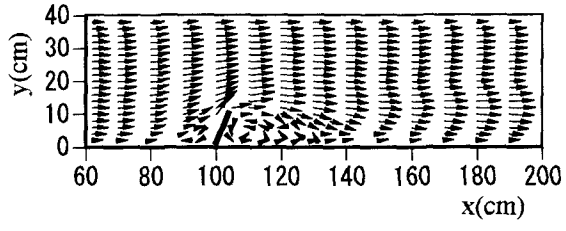

(b) Simulation (z=1cm)

Fig.10 120-degree spur-dike

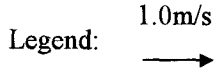

(2) Velocity distribution and large eddies

a) The inclined plane

On the side of spur-dike, the velocity is influenced directly by spur-dikes. From x=80cm to x=100cm the velocity decreases due to the blocking of spur-dike. For the condition of 60-degree spur-dike (see Fig.9), there is an eddy existing and also the reattachment length is about 20cm for both experiment and simulation. For the condition of 120-degree spur-dike (see Fig.10), there is an eddy downstream the spur-dike for both experiment and simulation. The reattachment length is about 20cm for experiment and the retachment length of

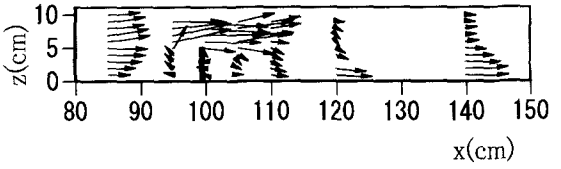

(a) Experiment (y=4cm)

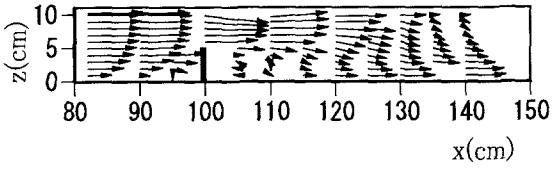

(b) Simulation (y=4cm)

Fig.11 60-degree spur-dike

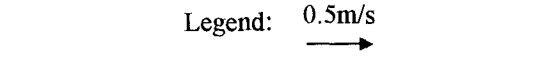

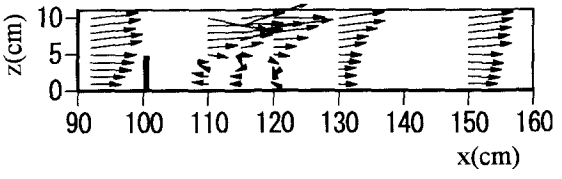

(a) Experiment (y=4cm)

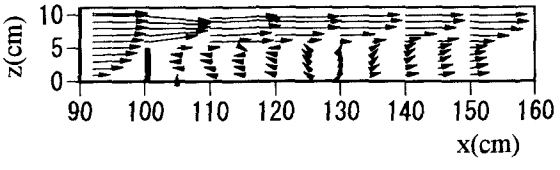

(b) Simulation (y=4cm)

Fig.12 120-degree spur-dike

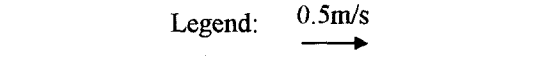

simulation is almost similar with that of experiment. From the reattachment point to the downstream on the side of spur-dike, the velocity distribution of simulation is a little different from that of experiment.

b) The longitudinal section

When the part of main flow crosses the submerged spur-dike, the flow area increases. Then an eddy appears in the longitudinal section. For the condition of 60-degree spur-dike (see Fig.11), the eddy size of experiment is smaller than that of simulation. For simulation, the eddy is about 10cm long. From the reattachment point to the downstream, the water surface velocity decreases sharply while bed surface velocity increases greatly for both experiment and simulation. For the condition of 120-degree spur-dike (see Fig.12), the eddy size is about 25cm long for experiment and 30cm long for simulation. The bed surface velocity decreases and the numerical

result is more serious than the experimental one.

Moreover the surface velocity with the condition of 60-degree spur-dike decreases drastically to very small values downstream of spur-dike while that with the condition of 120-degree spur-dike doesn't change remarkably downstream of spur-dike.

c) Cross-section

For the condition of 60-degree spur-dike, the eddy size and shape of simulation is almost the same with that of experiment; the width of eddy is about 15cm (see Fig.13). For the condition of 120-degree spur-dike, the flow structure is complex and the flow direction is chaotic for both experiment and simulation (see Fig.14).

6. CONCLUSIONS

It is proved that LES is an effective tool to simulate the three-dimensional flow around the submerged spur-dike. The numerical method is established on the base of finite-volume/finite-difference method with staggered grid. It is an improvement on MAC method and can deal with the problems of free surface and complex boundaries using the equivalent Cartesian grid method. The numerical results are in agreement with the experimental ones on the whole. Therefore, the equivalent Cartesian grid method can provide an accurate simulation of incompressible flow over complex boundaries and it is also not difficult to apply the method to the 3-dimensional flow with regular boundaries.

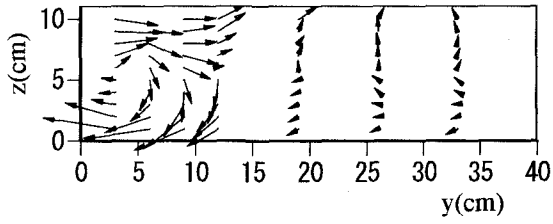

(a) Experiment (x=120cm)

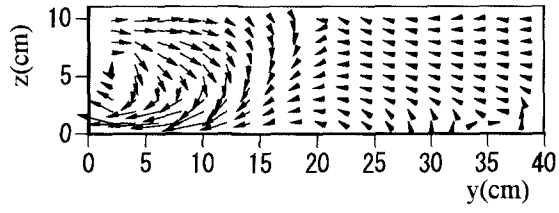

(b) Simulation (x=120cm)

Fig.13 60-degree spur-dike

Legend: 0.5m/s

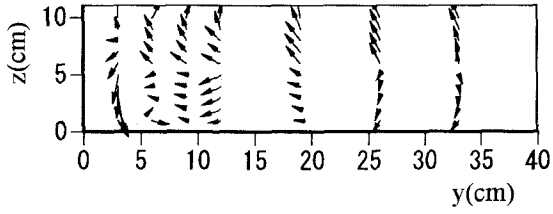

(a) Experiment (x=130cm)

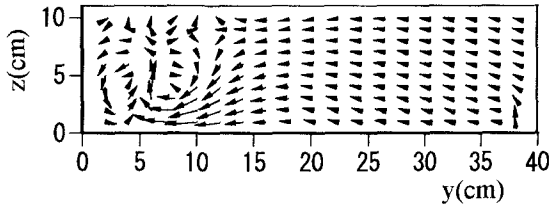

(b) Simulation (x=130cm)

Fig.14 120-degree spur-dike

Legend: 0.5m/s

REFERENCES

1) Hinokidani, O.: *Study on the 3-D flow of lake and river with 2-D bed evolution,* Doctoral Dissertation submitted to Kyoto University, 1992.
2) Mayerle, R., Toro, F. M. and Wang, S. S. Y.: Verification of a three-dimensional numerical model simulation of flow in the vicinity of spur-dikes, *J. Hyd. Res.,* Delft, The Netherlands, vol.33, No.2, pp243-256, 1995.
3) Peng, J. and Kawahara, Y.: Application of linear and non-linear k-ε models to flows around spur-dikes, *Annu. J. of the Hyd. Eng., JSCE,* pp643-648, 1998.
4) Floryan, J. M. and Rasmussen, H.: Numerical methods for viscous flows with moving boundaries, *Appl. Mech. Rev.,* vol. 42, pp.323-340, 1989.
5) Rodi, W.: Large-eddy simulation and statistical turbulence models: Compementary approaches, *New tools in the turbulence modeling,* Springger, 49-72, 1996.
6) Leisure, M.: *Turbulence in fluids,* Kluwer Academic publishers, pp322, 1990.
7) Smagorinsky, J.: General circulation experiment with the primitive equations, (1) The basic experiment, *Mon. Weath. Rev.,* vol.91, No.3, pp.99-164, 1963.
8) Harlow, F., H. and Welch, J. E.: Numerical calculation of time-dependent viscous incompressible flow of fluid with free surface, *Phys. Fluids,* Vol. 8, pp2182-2189, 1997.
9) Nichols, B. D. and Hirt, C. W.: Improved free surface boundary conditions for numerical incompressible-flow calculation, *J. Comp. Phys.,* Vol. 8, pp434-448, 1971.
10) Nakatsuka, K.: *A large-eddy simulation model of 3-dimensional flow around submerged spur-dike,* Thesis of Bachelor Degree submitted to Tottori University, Japan, 1999.
11) Van Driest, E. R.: On turbulent flow near a wall, *J. Aero. Sci.,* 1956.
12) Michiue, M., Hinokidani, O., Emad, E and Yamaguchi, N.: Experimental study of 3-D flow around submerged spur-dikes, *Proc. Of the Annu. Conf. of JSCE (Chugoku Branch),* pp181-182, 1999.

(Received September 30, 1999)